Technical Report

Spectral Imaging Using a Liquid Crystal Tunable Filter – Part II

Farhad Moghareh Abed and Roy S. Berns

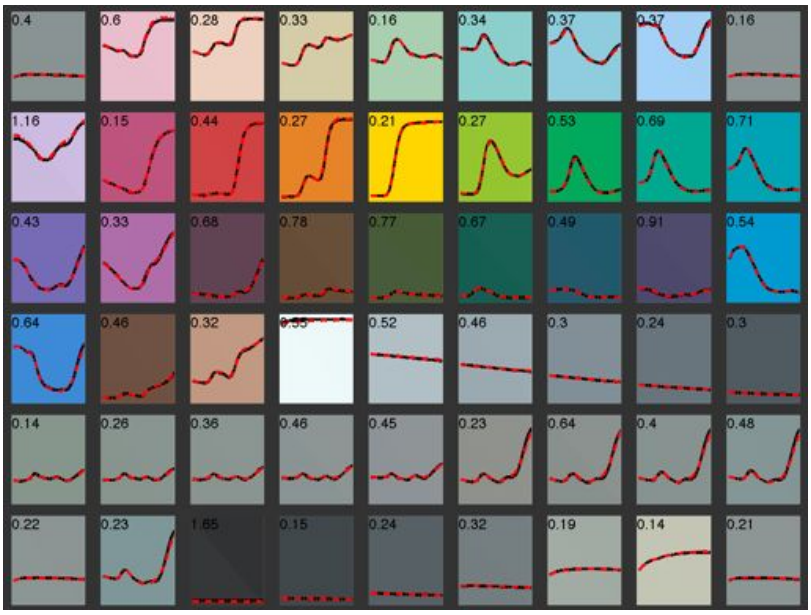

August 2014

R·I·T Rochester Institute of Technology
College of Science / Program of Color Science
Studio for Scientific Imaging and Archiving of Cultural Heritage
PoCS MCSL

1. Abstract

A practical workflow was developed for the spectral calibration of a liquid crystal tunable filter (LCTF) based multispectral imaging system. The goal was to acquire sufficiently accurate spectral information per pixel for pigment identification of paintings. Therefore, the Robertson-Robertson-Berns-Petersen based spectral correction algorithm was applied to the spectral signals following corrections for dark current, optical flare, camera response linearity, and flat-fielding. An additional spectral correction step was added to the calibration workflow to compensate for angular dependency of LCTF transmissions. The spectral correction transformation was derived using 24 samples of a X-Rite Passport as training data. The accuracy of the system was evaluated using matte and glossy independent color targets. The final mean CIEDE2000 and spectral RMS values for the matte test target were 0.4 and 0.7%, respectively. The influence of the measurement geometry was studied utilizing glossy patches of the second color target that led to 0.8 mean CIEDE2000 and 0.6% mean spectral RMS. According to the results, the proposed calibration workflow performed well in spectral estimations of different types of materials after a simple geometry correction using the 24 matte patches of the X-Rite Passport.

2. Introduction

Spectroscopy is one of the feasible and non-invasive technologies that is popular particularly for analyzing works of art in museums. With the growth of acquisition technologies in the past decade, a full spectral scan of the entire scene rather than a few spots became possible with more affordable equipment. Spectral imaging is particularly applicable in analyzing, documenting, inpainting, and reproducing museum artwork [1-8]. Pigment identification of paintings is another field in which spectral images are beneficial. In pigment identification algorithms, the possible primary pigments of a given painting are estimated by exploiting analytical and historical information of the painting. Among available analytical measurements, spectral imaging is considered a preferred choice since it is non-invasive as well as further exclusive advantages for treatment and dissemination procedures [9-13]. However, pigment identification algorithms demand a certain level of spectral accuracy and precision for practical use [12].

Developing multispectral imaging technology started about 40 years ago in the astrophysics, remote sensing, and medical fields. This technology became more accessible after undergoing rapid developments from the early 1990s to be applicable in other fields of research such as art conservation and examination [1]. Visual Arts: Systems for Archiving and Retrieval of Images (VASARI) was one of the first projects supported in the late 1980s by the National Gallery in London together with a consortium of European universities, institutions, and companies for capturing digital images of artwork with the aim of evaluating possible changes in paintings on display or during transportation between museums [1, 2, 8]. The VASARI project was followed by the Methodology for Art Reproduction in Color (MARC) project in the mid-1990s with the goal of making high-resolution colorimetric copies of paintings. MARC II was an enhanced version of MARC with the aim of improving capturing speed, which was utilized for digital documentation of the entire collection of the National Gallery, London. However, MARC was limited to colorimetric measurement and reproduction without any multispectral capabilities [2, 8]. CRISATEL was the next generation of

multispectral imaging systems developed as a successor to the VASARI scanner with the capacity of producing digital images with a size of $12{,}000 \times 20{,}000$ pixels and imaging paintings up to 2×2 meters. The images were captured by horizontally displacing a CCD consisting of a vertically mounted 12,000 pixel linear array and 13 narrow-band interference filters for better estimation of spectral reflectance in the visible and infrared regions [2, 14-16]. Another scanner-based spectrophotometric imaging system for paintings, developed in Italy, was comprised of a scanning table, a monochrome CCD, and a spectrograph [17-20]. Development of a multi-spectral scanning system was also pursued at the University of Ferrara [21, 22]. Their acquisition system was equipped with 32 (10-nm band) interference filters mounted in front of a monochrome CCD camera and a high-resolution scanning table. At the typical rate of measurements, the acquisition time for a $1m^2$ painting was reported to be about nine hours. ENST was another center that investigated the efficiency of multispectral acquisition systems [23-26]. In the imaging system developed by Tominaga, *et al.* at Chiba University, multispectral data were obtained by varying the light source to enhance the measurement speed and remove registration issues [27-29]. However, such a system is not appropriate for imaging fluorescent objects.

The Munsell Color Science Laboratory (MCSL) at the Rochester Institute of Technology (RIT) is another active center in developing spectral acquisition systems. Three multispectral capturing systems have been developed and evaluated at MCSL: a narrow-band color filter wheel and achromatic sensor, liquid crystal tunable filter (LCTF) and achromatic sensor and a dual filtered RGB sensor [30]. The LCTF capturing system acquired the multispectral data employing a monochrome CCD camera in 31 bands [31, 32]. The filtered RGB system was based on a set of RGB values of a trichromatic camera combined with two optimized absorption filters [33, 34]. The development of a spectral framework in MCSL was followed by implementing mathematical techniques for preserving colorimetric fidelity of spectral images such as Matrix-R-based and *Labpqr* spectral reconstruction methods [35-38]. Berns and Imai [12] and Berns, *et al.* [11] investigated the application of a multi-channel imaging system for pigment identification and pigment selection for inpainting in a subtractive mixing space. The research continued by further investigation for high-resolution spectral capturing [35, 37, 40] and using pigment information of improving the spectral estimations [40-43].

Recently, a remote spectral imaging system was developed by Liang, *et al.* using a telescope for scanning the wall paintings referred to as Portable Remote Imaging System for Multispectral Scanning (PRISMS) [44]. Noticeable numbers of research in the multi-spectral capturing field indicate the importance and practical application of spectral imaging. However, only a few researchers have considered and evaluated the spectral imaging predictions as a tool for pigment identification of paintings.

The applicability of any acquisition system is as important as the prediction accuracy. For instance, a direct spectrophotometric measurement for each point of the painting is a possible way of acquiring high spectral and spatial resolution images. Nevertheless, direct spectral measurements require expensive and time-consuming processes for capturing spectral information of an entire painting limiting their applications in practice [4, 45].

Alternative sorts of methods subsample the spectral reflectance using fewer wide or narrow band filters or light sources. The specifications of the methods affect the

capturing traits in terms of the spectral and colorimetric accuracy, cost, speed, signal-to-noise ratio (SNR), complexity, and maintenance of the equipment. Ideally, the spectral factors can be estimated according to a characterized optical model and statistical inverse methods. However, full spectral characterization of all optical elements of the capturing necessitates advanced and expensive laboratory equipment. Target-based calibration methods are easy to implement, feasible, and affordable where the system parameters are derived according to a standard color target with known spectral reflectances.

This technical report describes research extending previous research of Hensley and Wyble [31] who developed a practical pipeline for target-based spectral estimation per pixel of paintings using a LCTF-based capturing system at MCSL. The previous research covered the geometry, set up and physical properties of the capturing system as well as a general overview of the spectral calibration workflow. This research mainly addresses the angular dependency of LCTF transmission and the geometry corrections for spectrophotometric and radiometric measurements.

3. Theory

3.1. Multispectral measurement

Spectral imaging systems measure spectral reflectance for each pixel. The number of components per pixel can be as few as three (such as a traditional RGB camera) to several hundred of bands for hyper-spectral images. In practical multispectral capturing systems, the spectral radiance of the scene is under-sampled into a lower dimensional space (usually four to 30 bands) according to the spectral sensitivity of device sensor, number, and transmission of the filters and spectral power distributing the light source(s). Any pixel is a vector of values representing projection of spectral radiance into a lower dimensional space. Statistically, increasing the number of channels provides more information of the surface spectral reflectance but required further measurement time and processing in addition to more advanced capturing equipment.

The next step is to estimate the reflectance factor according to the acquired camera signals, also known as spectral reconstruction. Most of the reconstruction algorithms consider a linear optical model and additive noise for the camera in which the acquisition responses are the integration of all the energy that reaches the sensor weighted by the sensitivity of each channel [25, 46-48]. The channel sensitivity is the result of filter transmission and the sensitivity of the detector. Once the model is defined, the reflectance factor can be estimated for each pixel using mathematical and statistical techniques. In target-based methods, the model parameters are derived using a set of known reflectance factors along with the corresponding camera responses.

3.2. Spectral Calibration

Initially, camera responses are processed to a fixed known state as a precursor to calibration [49]. Preparation of input and output data is more important in target-based methods because the model parameters are obtained directly from a set of standard input and output data. This sensitivity led to a number of studies [50-58], evaluating a number of factors affecting the accuracy of results regarding standard target structure and capturing hardware [23]. Checking for linearity of the detector, noise, dark current, and flat fielding can be some of the regular steps in calibrating CCDs. Extra correction might

be needed to associate with the spectral properties of the capturing systems such as transmittance shift of LCTF with incident angles reported and geometry differences [9, 14, 15, 31, 59].

As already mentioned, we considered a linear optical model for characterizing the capturing system. The mathematics of the optical model is shown in Eq. 1. This equation relates the camera response of *i*-th channel of the camera response (a_i) at 2-D position x [25, 46-48]:

$$a_i(x) = \int_{\lambda_1}^{\lambda_2} E(\lambda, x)\rho(\lambda, x)S_i(\lambda, x)d\lambda + e_i(x) \qquad (1)$$

The camera responses are defined as the integration of all the radiant energy that reaches the sensor weighted by the sensitivity of the channels (S_i). The channel sensitivity, S, is the result of filter transmission and the sensitivity of the detector. ρ and E are reflectance factor of the surface and the spectral power distribution of the light source, respectively. λ_1 and λ_2 determine the measurement wavelength range associated with the sensitivity of the sensor and filter transmissions. $e_i(x)$ is the measurement noise associated with the *i-th* channel at location x.

The goal is to estimate ρ in the Eq. 1. Among available methods of spectral estimation [3, 4, 25, 35, 47, 58, 60-63], we selected the Robertson-Berns-Petersen [64, 65] method due to the sufficient sampling of spectral radiance provided by the LCTF-based acquisition system. In other words, camera responses are considered as spectral data with different bandwidth and possible wavelength shift. Robertson and Berns and Petersen investigated and explained how these sorts of spectral differences can be taken into account and rectified. Using this method, the number of required coefficients reduces significantly compared to the other statistical methods implemented at MCSL such as pseudo-inverse [4]. The performances of Robertson-Berns-Petersen and matrix pseudo-inverse methods were investigated in the first technical report by Hensley and Wyble [31]. The correction equation for converting between two classes of reflectance factors (ρ_j from spectrophotometer and a_j from the acquisition system for *j-th* wavelength) is provided as follows:

$$\rho_j = \beta_{0,j} + \beta_{1,j}a_j + \beta_{2,j}\frac{da_j}{d\lambda} + \beta_{3,j}\frac{da_j^2}{d^2\lambda} \qquad (2)$$

Since the camera signal has been linearized in advance, the nonlinear terms were omitted from the original form of the Robertson-Berns-Petersen equation. In addition, an extended form of the equation provided by Robertson-Berns-Petersen was used in which the β values were optimized as a function of wavelength because wavelength shift and channel bandwidths vary for each wavelength [31]. This idea of using the wavelength-based spectral correction for spectral imaging purposes also was first used by Mohammadi and Berns for spectral imaging using a six channel capturing system [67]. The models coefficients are estimated using linear regression.

Considering the optical model presented in Eq. (1), the camera responses must be corrected for linearity, dark current, and optical flare in advance. The linearity of the camera response with the incoming radiance can be evaluated and corrected by a set of non-selective grey samples [59]. Dark current is defined as the sensor readings when no incident light exists. The dark current of the camera is measured by acquiring camera signal with the lens cap on. Flare causes unwanted increase of camera responses due to stray light to the camera lens. Opposed to dark current, flare varies with the scene content (e.g., flare is larger for senses with the bright background). Flare can be measured by

placing a black trap at the object plane; any non-zero signal (after subtracting dark current) defines flare. Therefore, the camera signals are corrected by subtracting the dark current and flare values from the camera as the preliminary calibration step.

The spectral measurements of different patches from regular spectrophotometers have constant illumination for all the samples; consequently, the target patches must be illuminated uniformly before being used in Eqs. 1 and 2. Since perfectly uniform illumination is not practical, further spatial correction is required. Additionally, camera lens fall-off still influences the uniformity of the captured image even in an ideal uniform illumination. The illumination non-uniformity as well as lens fall-off are addressed in the flat-field correction. In flat-fielding, a uniform lambertian surface is imaged. Since the incident radiance of a lambertian surface corresponds to the incident light energy, the captured image is a metric of camera fall-off and illumination non-uniformity. Eventually, the entire image is corrected to yield constant values for all locations in the image using a linear equation.

The corrected response after flat-fielding, dark current and flare correction are shown in Eq. 3.

$$a_{cr}(x) = \frac{a_{raw}(x) - a_{dc}(x) - (a_{fl} - a_{fl,dc})}{a_{ff}(x) - a_{dc}(x) - (a_{ff,fl} - a_{ff,dc})} \qquad (3)$$

In this equation, a_{raw} denotes the raw response of the camera. Subscripts *ff*, *fl* and *dc* are camera responses for flat-field, flare, and dark current images correspondingly. a_{cr} is the corrected camera signal.

Another spatial non-uniformity associated with the LCTF-based spectral systems is expected variability of the filter transmissions according to the incident light angle [15]. An example of this wavelength shift can be seen for a rendered image of a uniform solid red patch after flat-fielding (Figure 1). It can be seen that the visual color difference of different parts of the image is perceivable.

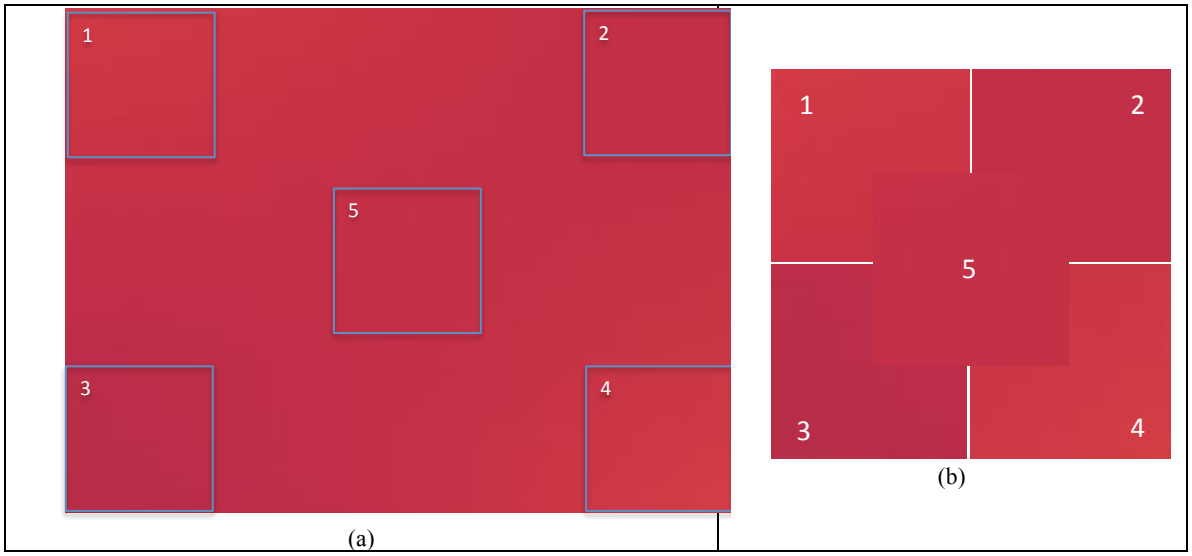

Figure 1: a) The rendered image of a red solid sample after spectral reconstruction with no angular correction. Captured using LCTF multispectral imaging system at MCSL. b) different samples of the image in five locations of the image specified in the original image (a).

In this research, we took the angular non-uniformity into account by using six solid uniform color sheets and the Robertson-Berns-Petersen spectral correction method. The

correction is done by dividing the image to smaller segments, *s*, since the incident angle can be written as a function of pixel location in the image. Accordingly, the aim was to obtain the same responses for all the segments for the uniform solid color patches. The corrections for each segment were performed using the following equation:

$$a_{s,i} = \gamma_{0,s,i} + \gamma_{1,s,i} a_{cr,c,i} + \gamma_{2,s,i} \frac{da_{cr,c,i}}{d\lambda} + \gamma_{3,s,i} \frac{da_{cr,c,i}^2}{d\lambda} \qquad (4)$$

In this equation, $a_{cr,c}$ is the camera response for segment *s* at the center of the image after flat-fielding and dark/flare corrections. $a_{s,i}$ are corrected responses for angular dependency of the measurements. γ coefficients are optimized for each segment so that the camera signal is equal to those at the center of the image for all uniform solid patches. Again, γ values are functions of the acquisition channel because the angular dependency is different per channel. Eventually, the camera responses are interpolated to match the wavelength range of the training spectral data in a separate step to be used in Eq. (2) (a_i to a_j).

In the last section of the experiments, the effect of measurement geometry on the spectral estimation was evaluated. The geometry correction applied to the calibration process for a set of glossy patches and according to the method introduced in Ref. [59].

4. Experimental

The research was conducted using the LCTF-based spectral imaging system at Munsell Color Science Laboratory (MCSL). Two metal-halide light sources (Buhlite Soft Cube light Sc-150) at almost 45° from the normal were used for illumination. The LCTF capturing unit was placed at the normal axis of the target surface (Figure 2). This geometry was most similar to the recommendation by ISO17321 (Section 4.3.3) for target-based illumination geometry [67]. A 1.4 megapixel Lumenera LW165m monochrome camera with a Sony ICX285 2/3' format 9.0x6.7 mm array sensor was used for image acquisition. A CRI Varispec LCTF was utilized for spectral filtration in 29 spectral bands from 435 to 700 nm. Each of the images is the average of ten measurements for each channel. The exposure time for each band adjusted to achieve 80% signal strength for the white sample. For more technical information about the measurement and hardware characteristics of the acquisition system, see [31].

The dark current and optical flare images were taken by putting on the camera cap and placing a light trap in each scene, respectively. We used a light trap made for dark calibration of the Color-Eye 7000 spectrophotometer. Since the optical flare is variable from scene to scene, the optical flare correction was carried out for each image. Afterwards, the collected images were flat-fielded for correcting lighting non-uniformities and lens fall-off using a flat uniform surface of Fluorilon (with the surface close to that of a Lambertian).

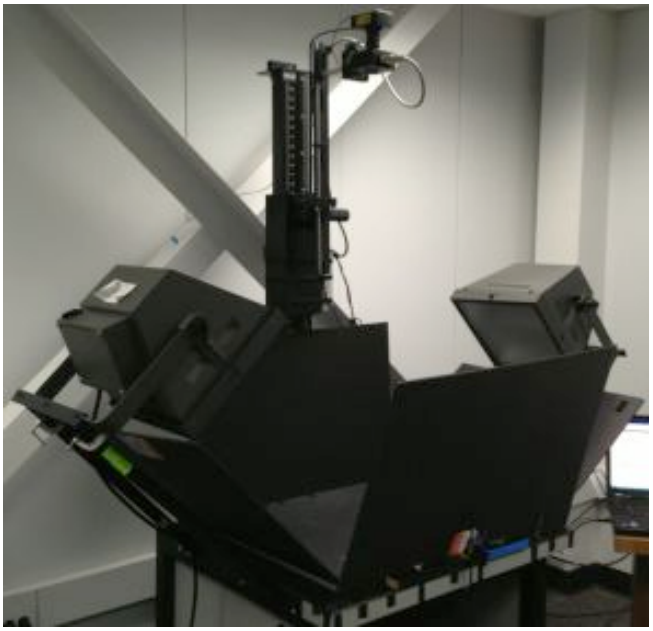

Figure 2: The LCTF-based capturing unit at MCSL.

Six sheets of uniform solid matte Color-aid paper mounted on foamcore were used to correct for angular changes. Spectral reflectances of the solid samples illustrate that they have enough variation in different spectral regions to calculate correction coefficients (Figure 3). The γ values in Eq. 4 were estimated using linear regression using the data for these six samples.

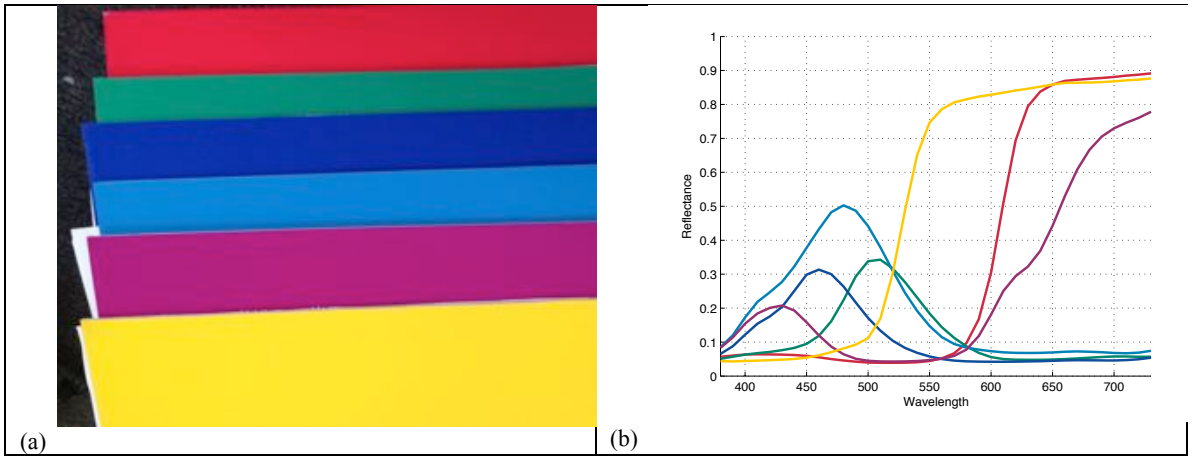

Figure 3: Uniform solid sheets used for angular correction. a) six uniform chromatic sheets b) the spectral reflectance of the uniform samples.

The linearity of the each one of the channels was examined using camera responses of the five gray samples of the ColorChecker Passport. The r-square of 1.000 for all 29 channels indicated excellent linearity of the camera signals to incident radiant light. Thus, no linearity correction was applied to the camera responses. However, this is an important factor that must be taken into account before using the data for spectral calibration.

Once the camera responses were corrected for dark current, flare, linearity and illumination and the angular non-uniformities, β values were optimized in Eq. 2 using the

24 samples of a X-rite ColorChecker Passport (Figure 4). The ColorChecker Passport is a popular and accessible color target, used by photographers for common colorimetric calibration and adjustments. A paint color target (MCSL Spectral Target 1) was used for evaluating the calibration process (Figure 5). The color target contains different chromatic and achromatic patches, which cover the entire color space adequately. There are two series of gray samples in this color target. The first set is the mixture of titanium white and carbon black; whereas, another set is a mixture of chromatic pigments to evaluate the accuracy of the spectral estimation for metameric pairs. This combination of color patches made this paint target a perfect independent color target with reasonable spectral variations over a wide range of hue. The averaged camera responses of each color patch were used for the calculations.

Figure 4: ColorChecker Passport with 24 matte samples.

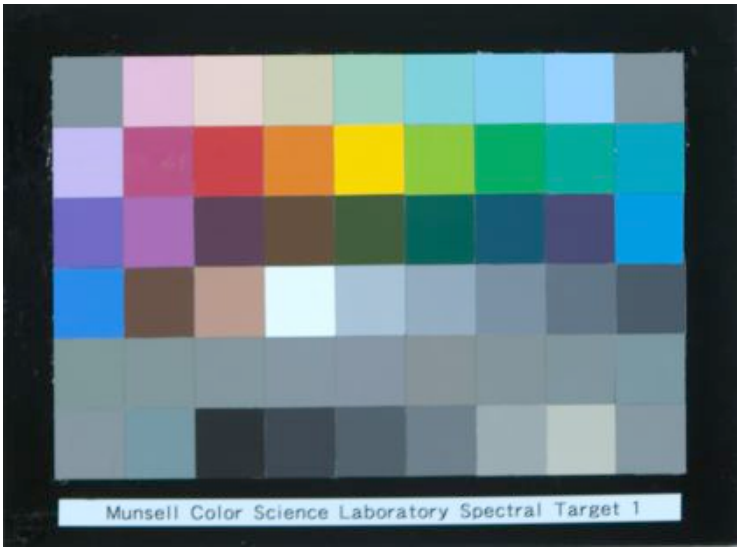

Figure 5: The MCSL paint target.

A second custom color chart comprised of 50 matte and 50 glossy patches was used or evaluating the geometry effect on the spectral calibration. Different patches were made by mixing Golden matte acrylic paints to achieve a reasonable color gamut, a set of neutral and dark patches, as shown in Figure 6. An automotive gloss coating was applied to half of the samples to generate the glossy surfaces (Figure 6 (b)). Since the MCSL

Spectral Target was already used for evaluating matte patches, only the 50 glossy patches of this target were utilized for geometry assessments. The dark patches in this target also are useful for evaluating geometry dependencies, which are more sensitive to geometry variations. A Photo Research PR-655 SpectroScan tele-spectroradiometer (PR-655) was used for the radiance measurements. The spectroradiometer was placed approximately at the same location as the acquisition camera. The reflectance factor of each patch was calculated using pressed polytetrafluoroethylene (PTFE) powder as the reference white. For all the color targets, the camera responses of each color patch were extracted by averaging the pixel values by considering approximately 50% of the sample area from their centers.

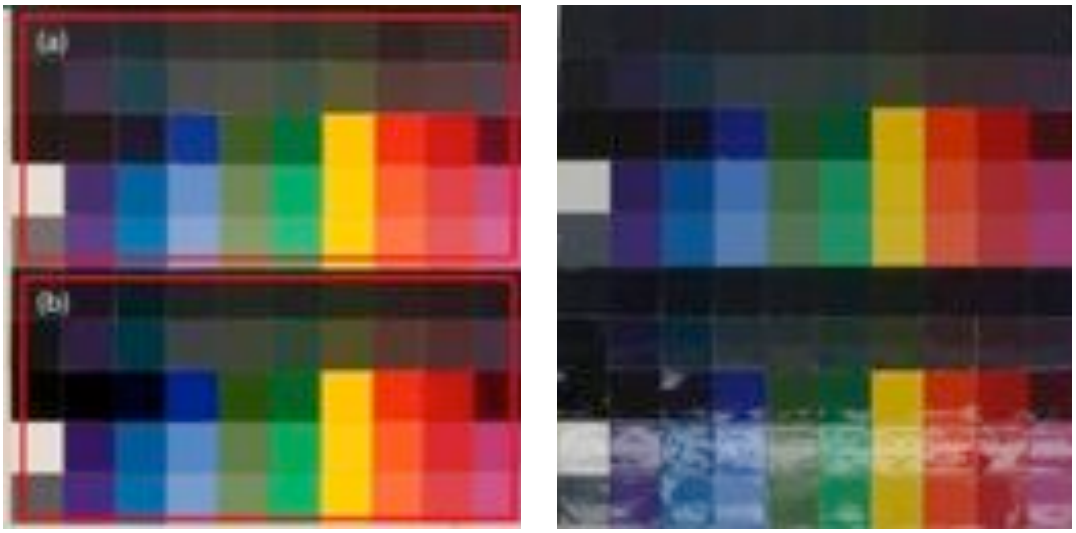

Figure 6: The custom color chart with 50 glossy and 50 matte patches viewed away from specular (left) and near specular (right) angles: (a) 50 matte patches, (b) 50 glossy patches.

5. Results and Discussion

The workflow of spectral calibration introduced in this research is depicted in Figure 7. As shown in the flowchart, all images are corrected for flare and dark current as preliminary steps before the next processes. Both flare and dark current subtractions were performed at the same exposure time for each channel. For flat fielding, the dark current-flare-corrected camera signals were divided to those of a flat-field image as shown.

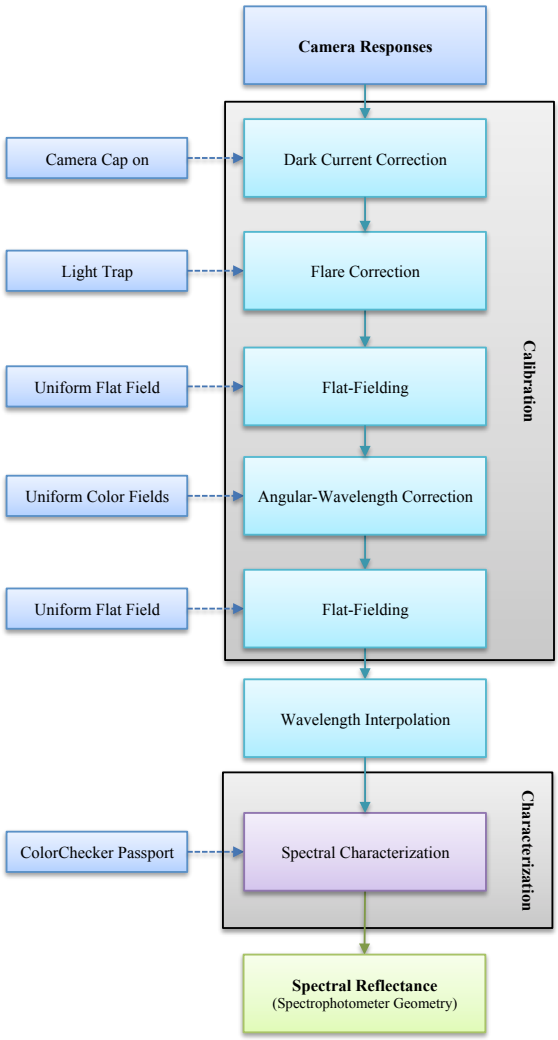

Figure 7: The general workflow of spectral calibration.

5.1. Angular Dependency

The next step is to evaluate and correct for angular dependency of the LCTF. The influence of filter transmittance shift for the red matte sheet is shown in Figure 8. It can be seen that the camera response changes toward the borders of the image due to the angular differences. The image at right is the histogram of the same image. Ideally, the camera responses must be similar for all the images if no wavelength shift exists.

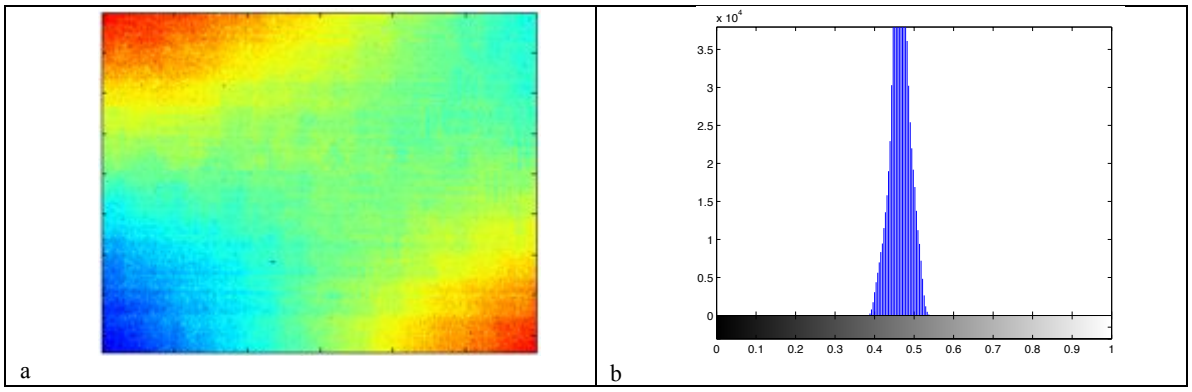

Figure 8: The non-uniformity of acquired data for red color sheet before correction (capturing channel corresponding to 611 nm). a) is a pseudo image showing non-uniformity of the red patch before correction. b) is the histogram of the same image.

This angular dependency can be quantized by calculating the color difference of different sections of the image compared to the central portion of the image for all six uniform solid sheets. Accordingly, the image was divided into 30x40 segments and CIEDE2000 calculated for each segment compared to central segment. The resulted mean and maximum CIEDE2000 values are plotted in Figure 9. The mean (max) CIEDE2000 of 0.95 (4.00) indicates significant angular changes in the LCTF-based system.

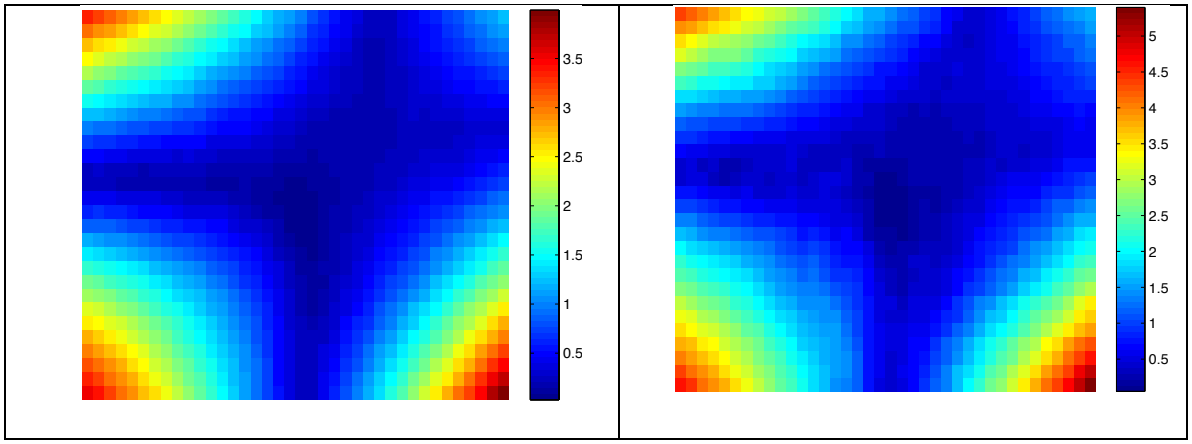

Figure 9: Mean (left) and maximum (right) CIEDE2000 for six color fields before the angular correction.

The result of angular correction for the same samples is shown in Figure 10 and

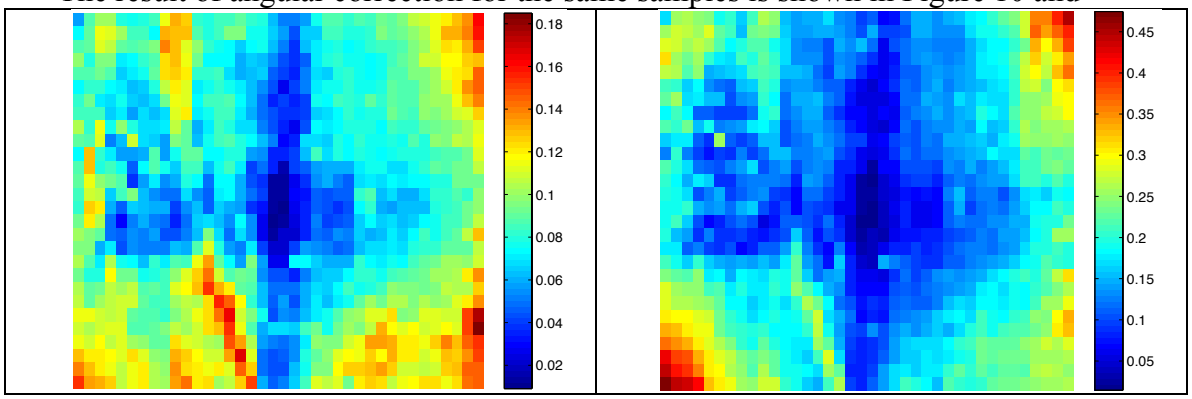

Figure 11. The mean and maximum of CIEDE2000 values after and before angular correction are summarized in Table 1. The mean (max) CIEDE2000 reduced to 0.08 (0.47) after correction. The color differences are still higher at the corners because the wavelength shift cannot be corrected by two neighboring camera responses. However, the uniformity of spectral values was significantly improved in the corrected images.

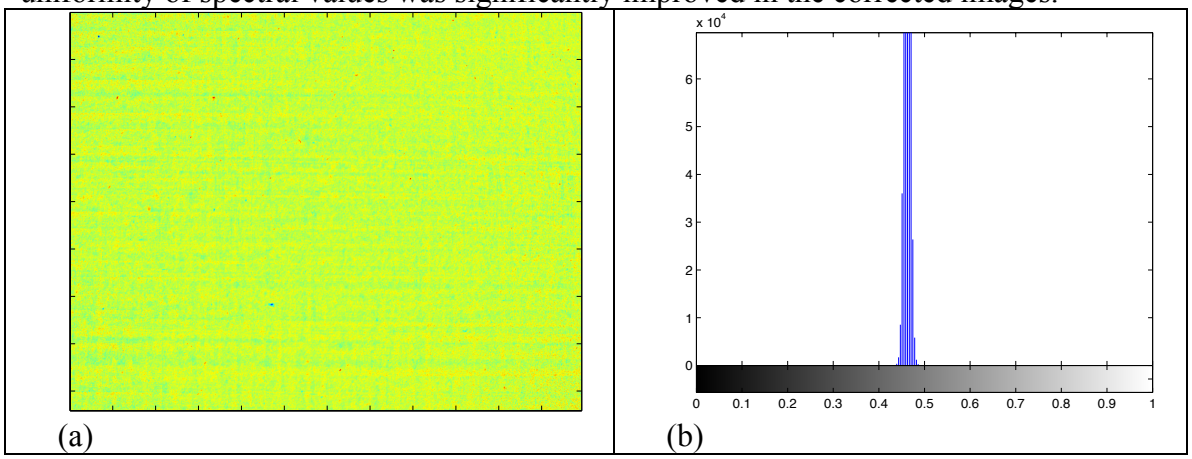

Figure 10: Non-uniformity of acquired data for red color field before correction (for the capturing channel corresponded to 611 nm wavelength). a) is a pseudo image showing non-uniformity of the red patch before correction. b) is the histogram of the same image.

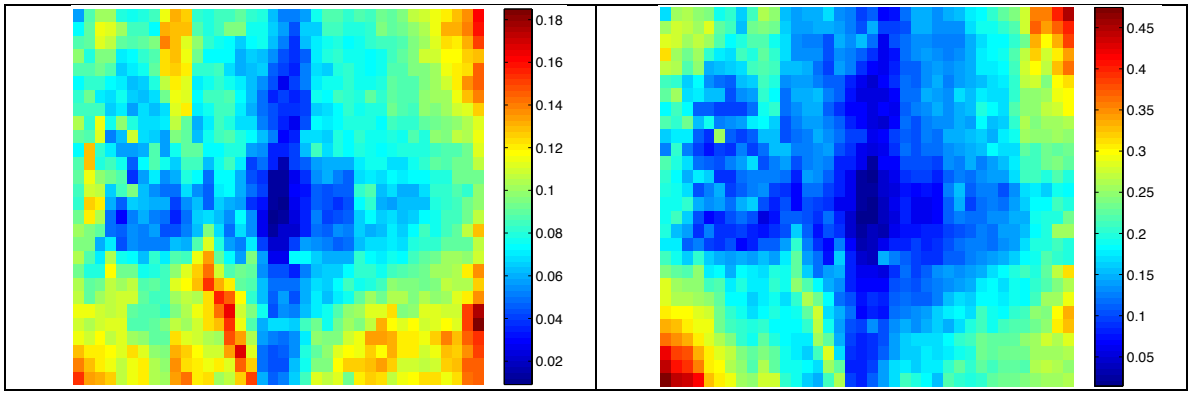

Figure 11: Mean (left) and maximum (right) CIEDE2000 for six color fields after correction.

Table 1: Mean and Maximum CIEDE2000 of segmented images of six solid color fields after and before correction.

		Before Correction	After Correction
Mean of Segments	Mean	0.95	0.08
	Max	4.00	0.18
Max of Segments	Mean	1.28	0.17
	Max	5.4	0.47

Another experiment was conducted in order to have a more standardized evaluation of the angular corrections. Consequently, the ColorChecker Passport was imaged in five different locations of the scene (Figure 12). CIELAB values of ColorChecker Passport were calculated for illuminant D65 and 1931 standard observer. The average CIEDE2000 values for 18 chromatic patches comparing color differences for all five positions before and after angular correction are shown in Tables 2 and 3. The grey samples removed

from the evaluation set because they do not have any wavelength-based modulations. The mean CIEDE2000 up to 1.82 expresses noticeable effect of the angular changes when the color checker is placed in two extreme corners of the scene. This error reduced to 0.51 after angular correction.

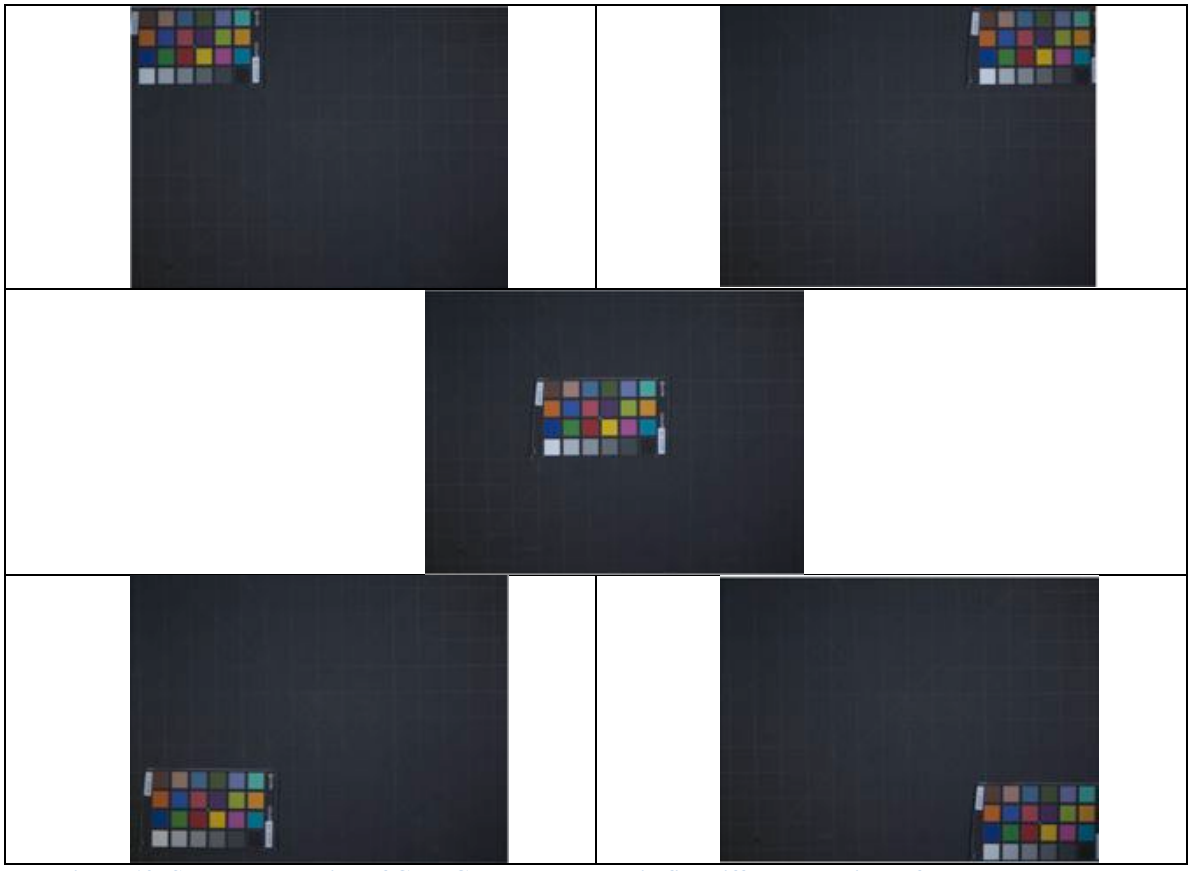

Figure 12: Spectral capturing of ColorChecker Passport in five different locations of the scene.

Table 2: The mean of CIEDE2000 values for chromatic patches of ColorChecker Passport in different locations of the scene before angular correction.

	Center	Up Right	Up Left	Down Right	Down Left
Center	0.00	0.50	0.49	1.36	1.32
Up Right	0.50	0.00	0.02	**1.82**	1.78
Up Left	0.49	0.02	0.00	1.81	1.77
Down Right	1.36	1.82	1.81	0.00	0.82
Down Left	1.32	1.78	1.77	0.82	0.00

Table 3: The mean of CIEDE2000 values for chromatic patches of ColorChecker Passport in different locations of the scene after angular correction.

	Center	Up Right	Up Left	Down Right	Down Left
Center	0.00	0.25	0.29	0.44	0.22
Up Right	0.25	0.00	0.35	0.42	0.25
Up Left	0.29	0.35	0.00	**0.51**	0.27
Down Right	0.44	0.42	0.51	0.00	0.41

Down Left	0.22	0.25	0.27	0.41	0.00

It is important to note that the angular correction experiment only needs to be performed once. After the coefficients are calculated, they can be used for later measurements. To keep the coefficient independency from measurement factors, another flat-field step was placed before the angular correction step in Figure 7. The next flat-fielding process is also required since wavelength correction might affect the previous flat-fielding corrections.

5.2. Spectral Calibration

The last step of the spectral calibration is to estimate the reflectance factor from the spatially corrected camera responses using Eq. 2. Before using the calibrated camera responses, an interpolation step is necessary for synchronizing the spectral wavelengths for the Robertson-Berns-Petersen spectral correction. Accordingly, the spectral images were interpolated considering the centroid wavelength of each channel (according to LCTF wavelength specifications) to be the same as wavelength intervals of the Eye-One spectrophotometer. Once the spectral images and spectral data from spectrophotometers had the same range of wavelength, Eq. (1) was used for final spectral predictions. Afterward, the β values in Eq. 2 were optimized using the 24 samples of the ColorChecker Passport. The results of spectral image of the ColorChecker Passport before and after calibration are shown in Figure 13. The colorimetric changes are also illustrated in Figure 14.

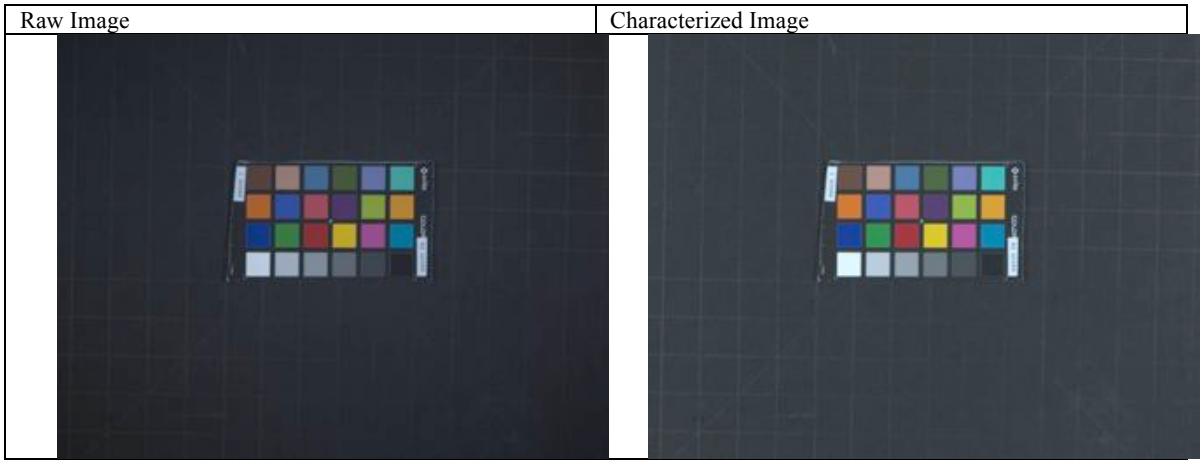

Figure 13: ColorChecker Passport before (left) and after (right) calibration process.

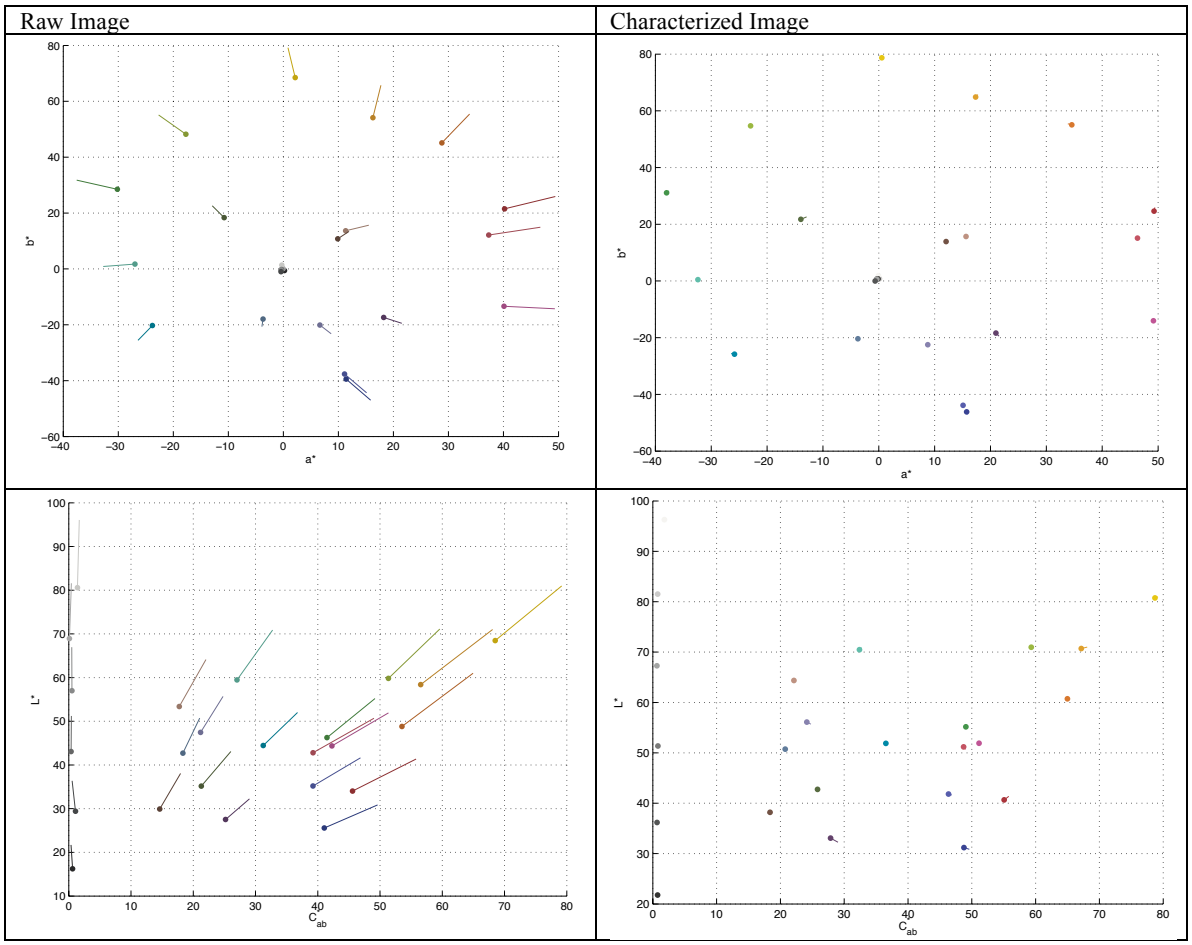

Figure 14: CIELAB values of the ColorChecker Passport in CIELAB color space (a*- L* and C*- L*) before (left) and after (right) calibration. In each plot, filled circles represent estimated values. The line connected to each circle shows the location of the actual value measured by eye-one spectrophotometer.

The estimated and measured reflectance factors are shown in Figure 15. The mean CIEDE2000 of all color patches of the training color target for each calibration step are shown in Table 4. The mean (max) CIEDE2000 of 0.45 (1.06) is an acceptable level of perceptual match between the estimated and measured data. The mean RMS of 0.00446 (~0.4%) is also a reasonable linear correlation between estimated and measured spectral reflectance factors, which is an important factor for pigment identification. According to the color differences in Table 4, the final spectral calibration led to a noticeable improvement to the estimations compared to simple interpolation after flat-fielding.

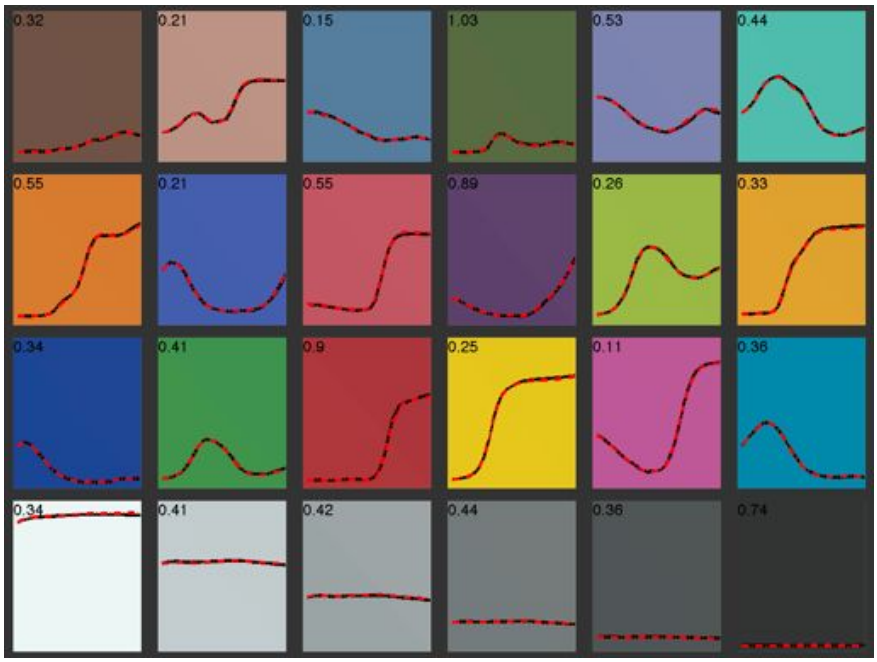

Figure 15: Actual (solid black) and estimated (dashed red) reflectance factors of the ColorChecker Passport patches. For each patch, the number at top-left corner indicates CIEDE2000 value between actual and predicted curves. The color of each sample is divided into two upper and lower triangles. The upper and lower triangles rendered corresponded to the predicted and actual reflectance factors respectively.

Table 4: CIEDE2000 and spectral RMS values between actual (from spectrophotometer) and the estimated reflectance factor of the ColorChecker Passport (training dataset) according to different calibration and calibration steps.

	CIEDE2000				Spectral RMS			
	Mean	Max	Variance	90p	Mean	Max	Variance	90p
Raw Image	8.01	11.95	4.45	10.13	0.11224	0.32312	0.00487	0.19348
Dark Corrected	8.09	12.01	4.33	10.19	0.11282	0.32381	0.00488	0.19405
Flare Corrected	8.27	12.14	4.02	10.33	0.11426	0.32545	0.00487	0.19544
Flat Fielded	1.25	2.24	0.34	1.95	0.01576	0.03829	0.00010	0.02932
Angular Corrected	1.32	2.20	0.32	2.03	0.01599	0.03859	0.00009	0.02866
Flat Fielded	1.31	2.11	0.35	2.07	0.01598	0.03931	0.00010	0.02940
Spectrally Characterized	**0.45**	**1.06**	**0.06**	**0.91**	**0.00446**	**0.00803**	**0.00000**	**0.00766**

The MCSL Spectral Target 1 was used as an independent dataset for validating the estimations. Consequently, the characterized spectral acquisition system (by the ColorChecker Passport) was used for estimating the reflectance factors of this target. The estimated and measured spectral reflectance factors are plotted in Figure 16. The mean (max) CIEDE2000 and RMS values are 0.4 (1.7) and 0.77% (2.5%) respectively. Similarity of color differences of training and independent color targets indicates that the calibration was not overfit to the test data. In other words, the calibration process is independent of the color target. The average CIEDE2000 and RMS for estimated spectral factor for the test color target are shown in Table 5. The results also emphasize the importance of the spectral calibration step compared to simple interpolation on flat-fielded images. If the flare and wavelength correction are omitted from the calibration

workflow, the average (max) CIEDE2000 and RMS values increase to 0.7 (1.8) and 0.96% (3.0%) respectively.

Looking at Figure 16, the largest CIEDE2000 value belongs to the black sample. The possible reasons are dissimilarities in the measurement's geometries and surface properties of the patches. In other words, geometrical difference between the reference spectrophotometer and the camera-taking capturing system lead to spectral differences if the surface structure of the evaluation target is different from those for the training target. In this case, if color patches of the MCSL Spectral Target 1 are not as matte as those of the ColorChecker Passport, the estimation might be slightly darker than the reference data. This hypothesis led to the next experiment for evaluating the effect of measurement geometry on the estimations.

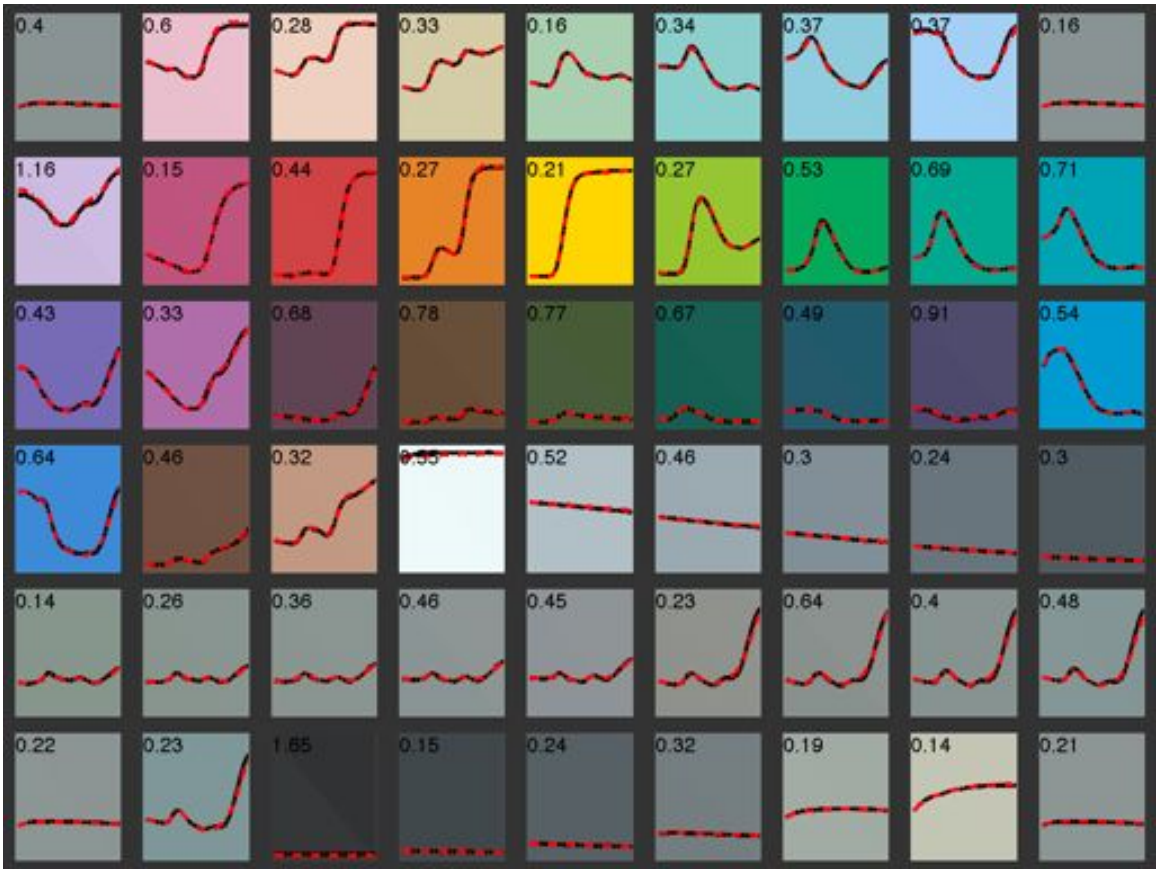

Figure 16: Actual (solid black) and estimated (dashed red) reflectance factors of the MCSL paint color target. For each patch, the number at the top-left corner indicates CIEDE2000 value between actual and predicted curves. The color of each sample is divided into two upper and lower triangles. The upper and lower triangles are rendered corresponded to the predicted and actual reflectance factors respectively.

Table 5: CIEDE2000 and spectral RMS values between actual (from spectrophotometer) and the estimated reflectance factor of the MCSL paint color target (independent dataset) according to different calibration and calibration steps.

	CIEDE2000				Spectral RMS			
	Mean	Max	Variance	90p	Mean	Max	Variance	90p
Raw Image	10.68	17.67	10.87	15.08	0.15294	0.33332	0.00722	0.27145
Dark Corrected	10.76	17.77	10.81	15.16	0.15353	0.33392	0.00722	0.27207
Flare Corrected	11.29	18.48	10.47	15.80	0.15770	0.33821	0.00722	0.27652
Flat Fielded	1.01	3.36	0.32	1.67	0.01944	0.05543	0.00019	0.04191
Angular Corrected	1.06	3.35	0.34	1.74	0.02014	0.04948	0.00020	0.04297
Flat Fielded	1.04	3.33	0.34	1.59	0.02028	0.05223	0.00021	0.04282
Spectrally Characterized	**0.44**	**1.65**	**0.07**	**0.71**	**0.00774**	**0.02539**	**0.00004**	**0.01820**

6. Geometry Dependency

As explained above, the influence of measurement geometry on calibration was evaluated according to previous research by the authors [59]. Accordingly, the estimated spectral reflectances were compared with those of a spectroradiometer. The training dataset was kept the same as previous experiments (reflectance factors of 24 ColorChecker Passport measured by x-rite Eye-one spectrophotometer). The results are shown in Table 6. The average CIEDE2000 was improved from 1.5 to 0.8 after geometry correction. The average and maximum spectral RMS values are similar to the results from the MCSL Spectral Target 1 (mean and maximum of 0.6% and 2.0%). This similarity of spectral RMS values shows the same accuracy in spectral estimations even though the average CIEDE2000 is rather larger due to the large number of dark sample in the second color target. The results of the spectral predictions after and before geometry correction are also illustrated Figure 17. The improvements mostly involved dark samples, which are more sensitive to geometry differences. In summary, the geometry-corrected spectral calibration is still valid for other sorts of materials and is independent of the surface structure. The third row of Table 6 (*self Trained*) shows the error values when 50 glossy samples of the custom color target are used for training and testing dataset as the minimum achievable error. A part of the error using this color checker can also be due to the dark samples having greater image noise. The slight geometry difference between the multispectral camera and the spectroradiometer measurement can be another source of error after geometry corrections.

Table 6: CIEDE2000 and spectral RMS values between the actual (from spectrophotometer) and the estimated reflectance factors of the 50 glossy samples of a custom color target for before and after geometry correction.

	CIEDE2000				Spectral RMS			
	Mean	Max	Variance	90p	Mean	Max	Variance	90p
Regular Calibration	1.51	4.25	0.51	2.32	0.01000	0.02601	0.00003	0.01668
Geometry Corrected	0.79	2.63	0.24	1.37	0.00649	0.02328	0.00003	0.01396
Self-Trained	0.60	1.97	0.19	1.19	0.00455	0.01464	0.00001	0.00841

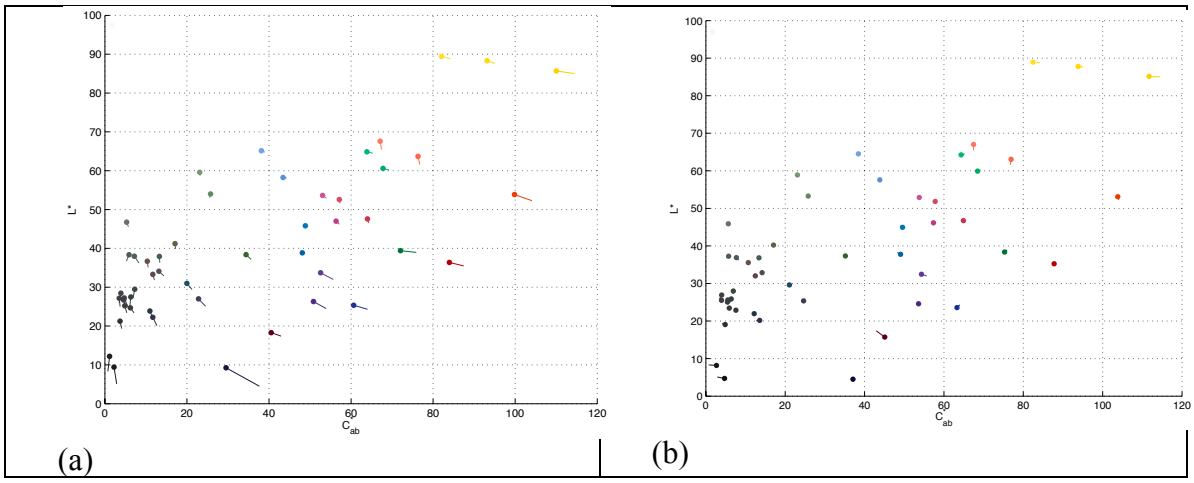

Figure 17: CIELAB values of the custom color chart patches calculated from actual (measured by spectroradiometer) and estimated reflectance factor before (a) and after (b) geometry correction.

7. Conclusions

A practical workflow for calibrating an LCTF-based, multi-spectral acquisition system was developed. In this research, the calibration workflow was based on a set of standard samples with known reflectance factors measured by a spectrophotometer. The camera responses were prepared in terms of dark current, linearity, flare, and angular non-uniformity of the LCTF transmissions. The angular correction was performed based on a set of matte solid color sheets by segmenting the image and utilizing the Robertson-Berns-Petersen spectral correction method for each segment and camera channel. Once the camera responses were corrected, they were used for deriving the model parameters for estimating reflectance factors of a standard color target. The calibration model was also based on the Robertson-Berns-Petersen spectral correction method.

The process was evaluated using two independent color targets. The first color target was comprised of 54 matte patches. According to the results, calibration led to similar spectral RMS and CIEDE2000 errors as the training data. In other words, the calibration model was not over-fitted to the training data.

Opposed to the matte samples used for training the camera model, the second color target was comprised of 50 glossy samples. The geometry dependency of the calibration was performed by comparing the estimated reflectance factors of the glossy patches of the second color target to those measured using a spectroradiometer. According to the result, the spectral estimations improved after correcting for the geometry dissimilarities.

Rather small CIEDE2000 and RMS values of the estimation indicate that the proposed method provides accurate enough data for the pigment identification goals. The geometry independency of the model is applicable when the painting does not have the same surface property as the training color target.

8. References

[1] C. Fischer and I. Kakoulli, "Multispectral and hyperspectral imaging technologies in conservation: current research and potential applications," *Studies in Conservation,* vol. 51, pp. 3-16, 2006.

[2] L. W. MacDonald, *Digital Heritage: Applying Digital Imaging To Cultural Heritage Preservation*: Routledge, 2006.
[3] S. Bianco, A. Colombo, F. Gasparini, R. Schettini, and S. Zuffi, "Applications of spectral imaging and reproduction to cultural heritage," *Digital Imaging for Cultural Heritage Preservation: Analysis, Restoration, and Reconstruction of Ancient Artworks,* p. 183, 2011.
[4] R. S. Berns, "Color accurate image archives using spectral imaging," *Scientific Examination of Art: Modern Techniques in Conservation and Analysis,* pp. 105-119, 2005.
[5] B. H. Berrie, "Rethinking the History of Artists' Pigments Through Chemical Analysis," *Annual Review of Analytical Chemistry,* vol. 5, pp. 441-459, 2012.
[6] V. Cappellini and A. Piva, "Opportunities and Issues of image processing for cultural heritage applications," in *Proc. EUSIPCO*, 2006.
[7] M. Barni, A. Pelagotti, and A. Piva, "Image processing for the analysis and conservation of paintings: opportunities and challenges," *Signal Processing Magazine, IEEE,* vol. 22, pp. 141-144, 2005.
[8] K. Martinez, J. Cupitt, D. Saunders, and R. Pillay, "Ten years of art imaging research," *Proceedings of the IEEE,* vol. 90, pp. 28-41, 2002.
[9] S. Baronti, A. Casini, F. Lotti, and S. Porcinai, "Multispectral imaging system for the mapping of pigments in works of art by use of principal-component analysis," *Applied optics,* vol. 37, pp. 1299-1309, 1998.
[10] S. Bruni*, et al.*, "Field and laboratory spectroscopic methods for the identification of pigments in a northern Italian eleventh century fresco cycle," *Applied spectroscopy,* vol. 56, pp. 827-833, 2002.
[11] R. S. Berns, J. Krueger, and M. Swicklik, "Multiple pigment selection for inpainting using visible reflectance spectrophotometry," *Studies in conservation,* pp. 46-61, 2002.
[12] R. S. Berns and F. H. Imai, "The use of multi-channel visible spectrum imaging for pigment identification," 2002, pp. 217-222.
[13] H. Liang, K. Keita, B. Peric, and T. Vajzovic, "Pigment identification with optical coherence tomography and multispectral imaging," in *Proc. OSAV'2008, The 2nd I'ntl Topical Meeting on Optical Sensing and Artificial Vision*, 2008, pp. 33-42.
[14] A. Ribés, F. Schmitt, R. Pillay, and C. Lahanier, "Calibration and spectral reconstruction for crisatel: an art painting multispectral acquisition system," *Journal of Imaging Science and Technology,* vol. 49, pp. 563-573, 2005.
[15] H. Liang, D. Saunders, and J. Cupitt, "A new multispectral imaging system for examining paintings," *Journal of Imaging Science and Technology,* vol. 49, pp. 551-562, 2005.
[16] P. Cotte and D. Dupraz, "Spectral imaging of Leonardo Da Vinci's Mona Lisa: An authentic smile at 1523 dpi with additional infrared data," in *Proceedings of IS&T Archiving Conference*, 2006, pp. 228-235.
[17] G. Antonioli, F. Fermi, C. Oleari, and R. Riverberi, "Spectrophotometric scanner for imaging of paintings and other works of art," in *Proceedings of CGIV*, 2004, pp. 219-224.

[18] G. Novati, P. Pellegri, and R. Schettini, "An affordable multispectral imaging system for the digital museum," *International Journal on Digital Libraries,* vol. 5, pp. 167-178, 2005.
[19] P. Anna, R. Filippo, P. Luca, and C. Guido Maria, "Multispectral acquisition of large-sized pictorial surfaces," *EURASIP Journal on Image and Video Processing,* vol. 2009, 2009.
[20] N. Brusco*, et al.*, "A system for 3D modeling frescoed historical buildings with multispectral texture information," *Machine Vision and Applications,* vol. 17, pp. 373-393, 2006.
[21] P. Carcagni*, et al.*, "Spectral and colorimetric characterisation of painted surfaces: A Scanning device for the imaging analysis of paintings," in *Optical Metrology*, 2005, pp. 58570T-58570T-10.
[22] S. Ferriani, "A scanning device for multi-spectral imaging of paintings," 2006.
[23] F. Schmitt, H. Brettel, and J. Y. Hardeberg, "Multispectral imaging development at ENST," in *Proc. of International Symposium on Multispectral Imaging and Color Reproduction for Digital Archives*, 1999, pp. 50-57.
[24] J. Y. Hardeberg, "Multispectral color imaging," *To appear in NORSIGnalet,* 2001.
[25] J. Y. Hardeberg, *Acquisition and reproduction of color images: colorimetric and multispectral approaches*: Dissertation. com, 2001.
[26] J. Y. Hardeberg, F. Schmitt, and H. Brettel, "Multispectral image capture using a tunable filter," in *Color Imaging: Device Independent Color, Color Hardcopy and Graphic Arts*, 2000, pp. 77-88.
[27] S. Tominaga, "An approach to digital archiving of art paintings," in *Image Analysis*, ed: Springer, 2005, pp. 379-388.
[28] S. Tominaga, N. Tanaka, and T. Komada, "Imaging and rendering of oil paintings using a multi-band camera," in *Image Analysis and Interpretation, 2004. 6th IEEE Southwest Symposium on*, 2004, pp. 6-10.
[29] S. Tominaga, "CIC@20: Multispectral Imaging," presented at the Twentieth Color and Imaging Conference: Color Science and Engineering Systems, Technologies, and Applications, Los Angeles, California, 2012.
[30] F. H. Imai, M. R. Rosen, and R. S. Berns, "Multi-spectral Imaging of a van Gogh's Self-portrait at the National Gallery of Art, Washington DC," in *Is and ts pics conference*, 2001, pp. 185-189.
[31] B. Hensley and D. Wyble, "Spectral Imaging Using a Liquid Crystal Tunable Filter," 2012.
[32] F. Imai, L. Taplin, and E. Day, "Comparison of the accuracy of various transformations from multi-band images to reflectance spectra," 2002.
[33] F. H. Imai, D. R. Wyble, R. S. Berns, and D. Y. Tzeng, "A feasibility study of spectral color reproduction," *The Journal of imaging science and technology,* vol. 47, pp. 593-593, 2003.
[34] R. Berns, L. Taplin, M. Nezamabadi, M. Mohammadi, and Y. Zhao, "Spectral imaging using a commercial colour-filter array digital camera," 2005.
[35] Y. Zhao and R. S. Berns, "Image based spectral reflectance reconstruction using the matrix R method," *Color Research & Application,* vol. 32, pp. 343-351, 2007.

[36] R. S. Berns, L. A. Taplin, M. Nezamabadi, Y. Zhao, and Y. Okumura, "High-accuracy digital imaging of cultural heritage without visual editing," in *Proc. of IS&T's 2005 Archiving Conference*, 2005, pp. 91-95.
[37] Y. Zhao, L. Taplin, M. Nezamabadi, and R. Berns, "Using the matrix R method for spectral image archives," 2005.
[38] M. Derhak and M. Rosen, "Spectral colorimetry using LabPQR: an interim connection space," *Journal of Imaging Science and Technology,* vol. 50, pp. 53-63, 2006.
[39] Y. Zhao and R. S. Berns, "Predicting the spectral reflectance factor of translucent paints using Kubelka Munk turbid media theory: Review and evaluation," *Color Research & Application,* vol. 34, pp. 417-431, 2009.
[40] Y. Zhao, R. S. Berns, Y. Okumura, and L. A. Taplin, "Improvement of spectral imaging by pigment mapping," in *Color and Imaging Conference*, 2005, pp. 40-45.
[41] Y. Zhao, R. S. Berns, and L. Taplin, "Image segmentation and pigment mapping in spectral imaging," in *International Congress of Imaging Science ICIS'06*, 2006, pp. 294-297.
[42] Y. Zhao, R. S. Berns, L. A. Taplin, and J. Coddington, "An investigation of multispectral imaging for the mapping of pigments in paintings," *Proceeding of International Society for Optical and Photonics Engineering. San Jose: SPIE,* pp. 681007-1, 2008.
[43] Y. Zhao, *Image segmentation and pigment mapping of cultural heritage based on spectral imaging*: ProQuest, 2008.
[44] H. Liang, "Advances in multispectral and hyperspectral imaging for archaeology and art conservation," *Applied Physics A,* vol. 106, pp. 309-323, 2012.
[45] P. Geladi, H. F. Grahn, and J. Burger, "Multivariate images, hyperspectral imaging: background and equipment," *Techniques and applications of hyperspectral image analysis. Wiley, Chichester,* pp. 1-14, 2007.
[46] A. Ribes, R. Pillay, F. Schmitt, and C. Lahanier, "Studying that smile: A tutorial on multispectral imaging of paintings using the Mona Lisa as a case study," *Signal Processing Magazine, IEEE,* vol. 25, pp. 14-26, 2008.
[47] A. Ribes and F. Schmitt, "Linear inverse problems in imaging," *Signal Processing Magazine, IEEE,* vol. 25, pp. 84-99, 2008.
[48] H. Haneishi, T. Hasegawa, A. Hosoi, Y. Yokoyama, N. Tsumura, and Y. Miyake, "System design for accurately estimating the spectral reflectance of art paintings," *Applied Optics,* vol. 39, pp. 6621-6632, 2000.
[49] G. Sharma, *Digital color imaging handbook*: CRC, 2003.
[50] G. Hong, M. R. Luo, and P. A. Rhodes, "A study of digital camera colorimetric characterisation based on polynomial modelling," 2001.
[51] M. D. Fairchild, D. R. Wyble, and G. M. Johnson, "Matching image color from different cameras," *Symposium on Electronic Imaging: Science and Technology,* vol. 6808, pp. 68080E-68080E-10, 2008.
[52] V. Cheung, S. Westland, D. Connah, and C. Ripamonti, "A comparative study of the characterisation of colour cameras by means of neural networks and polynomial transforms," *Coloration technology,* vol. 120, pp. 19-25, 2004.

[53] F. M. Martínez Verdú, J. Pujol Ramo, and P. Capilla Perea, "Characterization of a digital camera as an absolute tristimulus colorimeter," *Proc. SPIE 5008, Color Imaging VIII: Processing, Hardcopy, and Applications,* 197-208 doi:10.1117/12.474876, 2003.

[54] K. Barnard and B. Funt, "Camera characterization for color research," *Color Research & Application,* vol. 27, pp. 152-163, 2002.

[55] V. Cheung, S. Westland, and M. Thomson, "Accurate estimation of the nonlinearity of input/output response for color cameras," *Color Research & Application,* vol. 29, pp. 406-412, 2004.

[56] C. Li, G. Cui, and M. R. Luo, "The accuracy of polynomial models for characterising digital cameras," *Proc. AIC Interim. Meet,* pp. 166-170, 2003.

[57] T. Cheung and S. Westland, "Color selections for characterization charts," 2004, pp. 116-119.

[58] D. Nyström, "Colorimetric and multispectral image acquisition using model-based and empirical device characterization," *Image Analysis,* pp. 798-807, 2007.

[59] F. M. Abed, R. S. Berns, and K. Masaoka, " Geometry-independent target-based camera colorimetric characterization," Journal Imaging Science Technology vol. 57, 050503-050501 – 050515 (2013).

[60] S. Peyvandi, S. Amirshahi, J. Nieves, and J. Romero, "Generalized Inverse-Approach Model for Spectral-Signal Recovery," 2013.

[61] F. M. Abed, S. H. Amirshahi, and M. R. M. Abed, "Reconstruction of reflectance data using an interpolation technique," *JOSA A,* vol. 26, pp. 613-624, 2009.

[62] H. S. Fairman and M. H. Brill, "The principal components of reflectances," *Color Research & Application,* vol. 29, pp. 104-110, 2004.

[63] M. R. Keenan, "Multivariate analysis of spectral images composed of count data," *Techniques and Applications of Hyperspectral Image Analysis,* pp. 89-126, 2007.

[64] A. R. Robertson, "Diagnostic performance evaluation of spectrophotometers," in *Advances in Standards and Methodology in Spectrophotometry*, C. Burgess and K. D. Mielenz, eds. (Elsevier, Amsterdam, 1987), pp. 277-286.

[65] R. S. Berns and K. H. Petersen, "Empirical modeling of systematic spectrophotometric errors," *Color Research & Application,* vol. 13, pp. 243-256, 1988.

[66] M. Mohammadi and R. S. Berns, "Diagnosing and correcting systematic errors in spectral-based digital imaging," in *Color and Imaging Conference*, 2005, pp. 25-30.

[67] ISO, "Graphic technology and photography -- Colour characterisation of digital still cameras (DSCs) Part 1," in *17321-1*, ed. Switzerland, 2006.